MESH TRANSFORMATION AND REGULARIZATION IN NUMERICAL SIMULATION OF AUSTENITIC-MARTENSITIC PHASE TRANSITION

ZHIPING LI

SCHOOL OF MATHEMATICAL SCIENCES, PEKING UNIVERSITY,
BEIJING 100871, P.R.CHINA

Abstract. A mesh regularization technique is developed in a numerical simulation of an austenitic-martensitic phase transition in which the mesh transformation method is applied to compute the martensitic transformation, the needle-like microstructures near the austenite-finely twinned martensite interface and the propagation of the austenite-finely twinned martensite interface. The numerical examples are given to show that the mesh transformation method equipped with the mesh regularization technique well simulates the development of twinned martensitic microstructures and the propagation of the austenite-finely twinned martensite interface.

1. Introduction

Many elastic crystals are known to undergo austenitic-martensitic phase transitions across the transformation temperature, when the higher symmetric phase (austenite) above the transformation temperature transforms to the lower symmetric phase (martensite), which often consists of fine mixtures of variants and exhibits microstructure, below the transformation temperature, and vice versa. Mathematical models and analysis based on the energy minimization have been developed to study the equilibrium state of phase transformations and microstructures [1]-[4]. Progress has also been made in developing numerical methods and analysis for these models (see [5]-[19] among many others).

1991 *Mathematics Subject Classification.* 73C50,65K10,65N30.

Key words and phrases. mesh transformation, mesh regularization, numerical simulation, phase transition, microstructure.

The research was supported in part by the Special Funds for Major State Basic Research Projects (G1999032802), NSFC and RFDP of China.

In the present paper, a numerical method based on the mesh transformation method [16, 17, 19] is developed to study the behavior of the austenitic-martensitic phase transition and the propagation of the austenite-finely twinned martensite interface as temperature varies. The choice of the mesh transformation method comes naturally from the observation that the numerical solutions of finite element approximations to the martensitic microstructures depend heavily on the mesh and a fixed mesh usually produces poor numerical results and can even lead to pseudo-microstructures [6, 7, 10, 14], and the mesh transformation method is successful in computing simple laminated microstructures and needle-like microstructures [16, 17, 19]. However, it is found that in some cases the energy minimizing procedure of the mesh transformation method forces some elements to be deformed into highly irregular shapes with the measure of the deformed elements almost vanishing, and it is also found that in computing needle-like microstructures by the mesh transformation method the elements near the tips of the long thin needles are often deformed into highly irregular shapes. The irregularity of the mesh then causes serious problem in computing the propagation of the microstructure. For instance, as the martensite needles grow into the austenite, the austenite needles shrink accordingly, however instead of withdrawing they only become thinner and thinner, and tend to shrink into the austenite line segments in the martensite. Although, theoretically speaking, shrinking into the line segments implies vanishing eventually, in computation, they do not easily vanish, and shrinking of the increasingly thin needle tips severely restricts the step size of the minimizing search and that eventually terminates the program before the minimizer is reached. Since the trouble is mainly caused by the irregularity of the deformed mesh, it motivates the development of the mesh regularization technique. The idea is that the numerical results produced by the mesh transformation method are projected on to a regular mesh to create regularized finite element approximations which are then taken as initial data for a new cycle of energy minimizing iteration using the mesh transformation method. The mesh regularization technique not only changes an ill-conditioned minimizing problem into a well-conditioned one by regularizing the mesh, but also helps to remove the extremely thin austenite needle tips which are supposed to vanish but still remained in the martensite and to break the energy barriers near the austenite-twinned martensite interface by introducing a relatively large perturbation in the neighborhood of the interface, where needle-like martensite microstructures form, so that the propagation of the interface can be well simulated. Numerical experiments showed that the mesh transformation method equipped with the mesh regularization technique works well and produces good numerical results for numerical simulation of the austenitic-martensitic phase transition.

The rest of the paper is arranged as follows. In section 2, a mathematical model for the problem of austenitic-martensitic phase transition is given. In section 3, the mesh transformation method with the mesh regularization technique is described. In section 4, numerical examples of the austenitic-martensitic phase transition and the propagation of the austenite-finely twinned martensite interface are presented and the numerical results are given and discussed to show the efficiency of the mesh transformation method combined with the mesh regularization technique.

2. A mathematical model

In the well known geometrically nonlinear theory of martensitic microstructures given by Ball and James [1, 2], microstructures are characterized by energy minimizing sequences which consist of increasingly fine oscillations and lead to Young measures of gradients [20]. For the static problem of austenitic-martensitic phase transitions, the theory leads to the consideration of minimizing an integral functional

$$F(u;\ \Omega) = \int_\Omega f(\nabla u(x),\ \theta(x))\, dx \tag{2.1}$$

in a set of admissible functions

$$\mathbb{U}(u_0;\ \Omega) = \{u \in W^{1,p}(\Omega; R^m) : u = u_0,\ \text{on } \partial\Omega_0\}, \tag{2.2}$$

where $\Omega \subset R^n$ is a bounded open set with a Lipschitz continuous boundary $\partial\Omega$, $\partial\Omega_0$ is a subset of $\partial\Omega$ with a positive $(n-1)$-dimensional measure, θ is a given temperature field and $1 < p < \infty$, and where the Ericksen-James elastic energy density $f(\cdot,\ \theta)$ is such that $f(\cdot,\ \theta)$ has a unique potential well above the transformation temperature ($\theta > \theta_T$) and has several symmetry related potential wells below the transformation temperature ($\theta < \theta_T$) [1, 2, 5, 21]. Since the Ericksen-James elastic energy density $f(\cdot,\ \theta)$ is required to be frame indifferent, it must be of the form [22, 21]

$$f(\nabla u,\ \theta) = \Phi(C,\ \theta), \tag{2.3}$$

where $C = (\nabla u)^T \nabla u \in \mathbb{S}^n = \{A \in R^{n\times n} : A^T = A\}$, which is the set of symmetric matrices in R^n, is the right Cauchy-Green strain tensor.

In the present paper, we consider a two dimensional model ($n = m = 2$) with

$$\Phi(C,\ \theta) = \frac{b(\theta)}{4}(C_{11} - C_{22})^2 - \frac{c(\theta)}{8}(C_{11} - C_{22})^2|C_{11} - C_{22}|$$
$$+ \frac{d(\theta)}{16}(C_{11} - C_{22})^4 + e\, C_{12}^2 + g(\operatorname{tr} C - 2)^2, \quad (2.4)$$

where

$$b(\theta) = (1 + \alpha \arctan \mu(\theta - \theta_T))d_0\hat{\varepsilon}^2, \quad (2.5)$$

$$c(\theta) = 2(1 + \frac{1 + 2\gamma}{3}\alpha \arctan \mu(\theta - \theta_T))d_0\hat{\varepsilon}, \quad (2.6)$$

$$d(\theta) = (1 + \gamma\alpha \arctan \mu(\theta - \theta_T))d_0, \quad (2.7)$$

and where $d_0 > 0$, $e > 0$ and $g > 0$ are the elastic moduli, $\hat{\varepsilon}$ is the transformation strain, θ_T is the transformation temperature,

$$\alpha \approx \frac{2}{\pi}, \quad \mu > 0, \ \text{and}\ \gamma < 1 \quad (2.8)$$

are the material constants used to reflect the change of elastic moduli and the energy barriers as the temperature varies.

Lemma 2.1. *Let $\Phi(C,\ \theta)$ be defined by (2.4), let*

$$C_{\varepsilon,\delta,\gamma} = \begin{pmatrix} 1 + 2\varepsilon + \delta & \gamma \\ \gamma & 1 + \delta \end{pmatrix} \quad (2.9)$$

and let $C_\varepsilon = C_{\varepsilon,-\varepsilon,0}$. Then, we have

$$\Phi(C_\varepsilon,\ \theta) \le \Phi(C_{\varepsilon,\delta,\gamma},\ \theta), \quad \forall\, \varepsilon,\ \delta,\ \gamma\ \in R^1 \quad (2.10)$$

and the equality holds if and only if $\delta = -\varepsilon$ and $\gamma = 0$.

Proof. A direct calculation by the definition of Φ gives

$$\Phi(C_{\varepsilon,\delta,\gamma},\ \theta) = \Phi(C_\varepsilon,\ \theta) + e\gamma^2 + 2g(\delta + \varepsilon)^2. \quad (2.11)$$

Since $e > 0$ and $g > 0$, the lemma follows. □

Lemma 2.2. *Let $\Phi(C,\ \theta)$ be defined by (2.4), then*

$$\Phi(C_0,\ \theta) \le \Phi(C,\ \theta), \quad \forall C \in \mathbb{S}^2, \quad \text{if}\ \theta > \theta_T, \quad (2.12)$$

where the equality holds if and only if $C = C_0$ which is the identity matrix I, and

$$\Phi(C_{\pm\hat{\varepsilon}},\ \theta) \le \Phi(C,\ \theta), \quad \forall C \in \mathbb{S}^2, \quad \text{if}\ \theta < \theta_T, \quad (2.13)$$

where the equality holds if and only if $C = C_{\pm\hat{\varepsilon}}$.

Proof. Since all $C \in \mathbb{S}^2$ can be written in the form of (2.9) and since $\Phi(C_{-\varepsilon},\ \theta) = \Phi(C_\varepsilon,\ \theta)$, by lemma 2.1, it only needs to show that (2.12) and (2.13) are satisfied for all $C = C_\varepsilon$ with $\varepsilon \geq 0$ for which we have

$$\Phi(C_\varepsilon,\ \theta) = b(\theta)\varepsilon^2 - c(\theta)\varepsilon^3 + d(\theta)\varepsilon^4. \tag{2.14}$$

Thus, by direct calculations on (2.14), it is easily verified that the conclusions of the theorem is true. $\square$

Figure 1 shows $\Phi(C_\varepsilon,\ \theta)$ as a function of ε for $\alpha = 2.02/\pi$, $\mu = 0.25$, $\gamma = 0$, $\hat{\varepsilon} = 0.05$, $d_0 = 500$ and various θ.

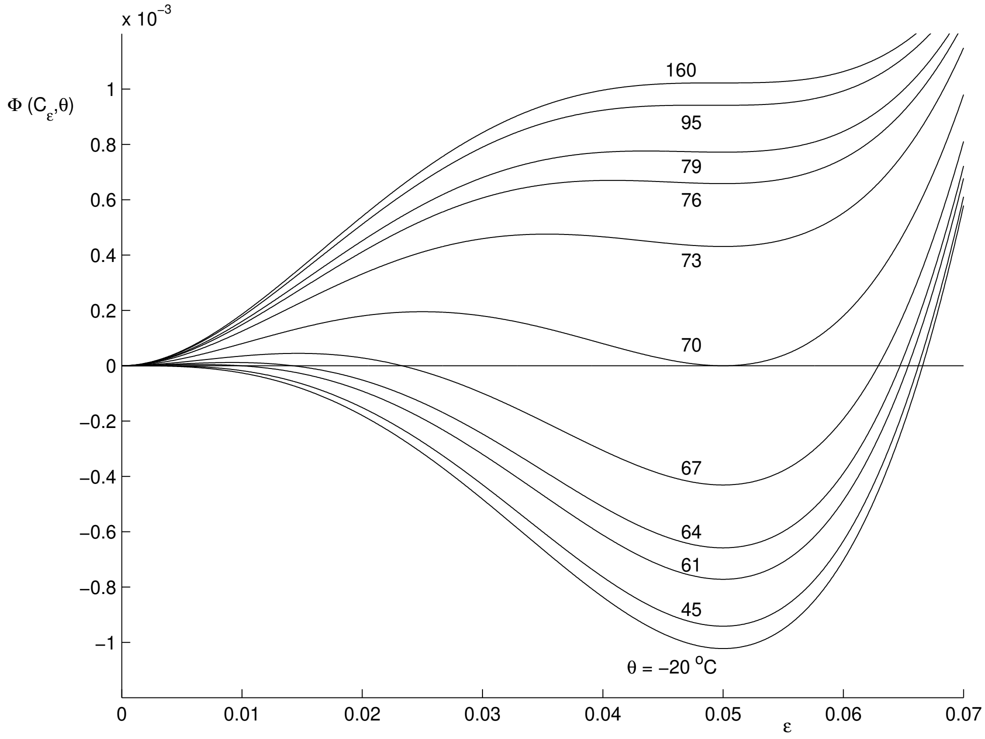

FIGURE 1. The energy density $\Phi(C_\varepsilon,\ \theta)$.

Theorem 2.1. *Let $\Phi(C,\ \theta)$ be given by (2.4). Then the energy density $f(\nabla u,\ \theta)$ defined by (2.3) has*

- **(i):** *a unique potential well $SO(2)$ for $\theta > \theta_T$;*
- **(ii):** *two symmetry related rotationally invariant potential wells $SO(2)U_0$ and $SO(2)U_1$ for $\theta < \theta_T$,*

where $SO(2)$ is the set of all 2×2 rotational matrices, and

$$U_0 = \begin{pmatrix} \sqrt{1-\hat{\varepsilon}} & 0 \\ 0 & \sqrt{1+\hat{\varepsilon}} \end{pmatrix}, \quad U_1 = \begin{pmatrix} \sqrt{1+\hat{\varepsilon}} & 0 \\ 0 & \sqrt{1-\hat{\varepsilon}} \end{pmatrix}. \tag{2.15}$$

Furthermore, U_0 and $R^{\pm}U_1$ are in rank-one connection. More precisely, let $\eta_1 = \sqrt{1-\hat{\varepsilon}}$ and $\eta_2 = \sqrt{1+\hat{\varepsilon}}$ and let

$$R^{\pm} = \begin{pmatrix} \eta_1\eta_2 & \pm\hat{\varepsilon} \\ \mp\hat{\varepsilon} & \eta_1\eta_2 \end{pmatrix}, \tag{2.16}$$

then, we have

$$R^{\pm}U_1 = U_0 + \mathbf{a}^{\pm} \otimes \mathbf{n}^{\pm}, \tag{2.17}$$

where $\mathbf{a}^{\pm} = \sqrt{2}\hat{\varepsilon}(\eta_1,\ \mp\eta_2)^T$ and $\mathbf{n}^{\pm} = \frac{1}{\sqrt{2}}(1,\ \pm1)^T$.

Proof. The conclusions (i) and (ii) follow directly from Lemma 2.2. The rest of the theorem can be verified by direct calculations (*c.f.* [1, 10]). □

The elastic energy density $\Phi(C,\ \theta)$ given above, of which the elastic moduli do not linearly depend on the temperature θ (compare [21]), has the advantages that (i) the temperature range during which the the transformation takes place can be adjusted by the parameter μ, the greater the μ the smaller the temperature range, (ii) the magnitude of the energy barriers for the phase transitions can be adjusted by the parameters α and γ, and (iii) the locations of the energy wells remain unchanged as the temperature varies.

While the energy minimizing sequence takes a crucial role in the computation of microstructures, especially in the computation of Young measures which give the probability distribution of the microstructure, the local minimizers of the the energy $F(u;\ \Omega)$ in $\mathbf{U}(u_0;\ \Omega)$ can also be of great importance, especially in the case, as in this paper, when the profile of needle-like microstructures near the austenite-finely twinned martensite interface is under consideration. It is such local minimizers which reveal the details of the needle-like microstructures near the austenite-finely twinned martensite interface that we are trying to compute with the method given in this paper.

3. Mesh transformation and regularization method

Let $\Omega \subset R^n$ be a bounded open set with a Lipschitz continuous boundary $\partial\Omega$, $\partial\Omega_0$ is a subset of $\partial\Omega$ with positive measure. Let $f : R^{mn} \to R^1$ be a continuous function which satisfies the following hypotheses for a constant $p > 1$:

(h1): $\max\{a_0, a_1 + b_1|\xi|^p\} \le f(\xi) \le a_2 + b_2|\xi|^p$,

(h2): $|f(\xi) - f(\eta)| \le C(1 + |\xi|^{p-1} + |\eta|^{p-1})|\xi - \eta|$,

where $a_0, a_1 \in R^1$, $a_2 > 0$, $b_2 \ge b_1 > 0$ and $C > 0$ are constants. Consider the problem of minimizing the functional

$$F(u;\ \Omega) = \int_\Omega f(\nabla u(x))\, dx \tag{3.1}$$

on a set of admissible functions

$$\mathbb{U}(u_0; \Omega) = \{u \in W^{1,p}(\Omega; R^m) : u(x) = u_0(x),\ \text{on } \partial\Omega_0\}. \tag{3.2}$$

Define

$$\begin{aligned} T(\Omega) = \{&\text{bijections } L : \bar\Omega \to \bar\Omega | L \in W^{1,\infty}(\Omega;\ R^m), L^{-1} \in W^{1,\infty}(\Omega), \\ &L(\partial\Omega_0) = \partial\Omega_0,\ \text{and } \det \nabla L > 0, a.e. \text{ in } \Omega\}. \end{aligned}$$

For any $L \in T(\Omega)$ and $u \in \mathbb{U}(u_0; \Omega)$, let $A \in R^{mn}$ and let $\bar u(x) : \Omega \to R^m$ be defined by

$$\bar u(x) = u(L(x)) - A\, L(x). \tag{3.3}$$

Then it is easily seen that $\bar u \in \mathbb{U}(\bar u_0; \Omega)$, where $\bar u_0(x) = u_0(L(x)) - A\, L(x)$,

$$\int_\Omega f(A + \nabla \bar u(x)(\nabla L(x))^{-1}) \det \nabla L(x)\, dx = F(u;\ \Omega), \tag{3.4}$$

and

$$\inf_{\bar u \in \mathbb{U}(\bar u_0; \Omega)} F(\bar u, L;\ \Omega) = \inf_{u \in \mathbb{U}(u_0; \Omega)} F(u;\ \Omega), \tag{3.5}$$

where

$$F(\bar u, L;\ \Omega) = \int_\Omega f(A + \nabla \bar u(x)(\nabla L(x))^{-1})) \det \nabla L(x)\, dx. \tag{3.6}$$

Let $\mathfrak{T}_h(\Omega)$ be regular triangulations of Ω with mesh sizes h [23]. Let

$$T_h(\Omega) = \{L \in T(\Omega) : L|_K \text{ is affine } \forall K \in \mathfrak{T}_h(\Omega)\}, \tag{3.7}$$

$$\mathbb{U}_h = \{u \in (C(\overline{\Omega}))^m : u|_K \text{ is affine } \forall K \in \mathfrak{T}_h(\Omega)\} \tag{3.8}$$

and

$$\mathbb{U}_h(v;\Omega) = \{u \in \mathbb{U}_h : u|_{\partial\Omega_0} = v\}. \tag{3.9}$$

Instead of finding a minimizer of $F(u;\ \Omega)$ in a fixed finite element function space $\mathbb{U}_h(u_0;\Omega)$, we solve the following discrete problem :

$$(MTM) \quad \begin{cases} \text{find } (u,\ L) \in \mathbb{U}_h(\bar{u}_0;\ \Omega) \times T_h(\Omega) \text{ such that} \\ F(u, L;\ \Omega) = \inf_{(u',L')\in\mathbb{U}_h(\bar{u}_0;\ \Omega)\times T_h(\Omega)} F(u', L';\ \Omega), \end{cases} \tag{3.10}$$

and use its solution $(\bar{u}_h,\ L_h)$ and the relation (3.3) to construct a finite element solution

$$u_h(x) = \bar{u}_h(L_h^{-1}(x)) + A\,x. \tag{3.11}$$

This is the so called mesh transformation method (for a more general form and the convergence analysis of the mesh transformation method, see [16, 17]), which by (3.3)-(3.5) is equivalent to minimizing the elastic energy $F(\cdot;\ \Omega)$ among all finite element function spaces introduced by $\mathfrak{T}_h(\Omega)$ and $T_h(\Omega)$ and thus is capable of producing much better numerical results than working on a fixed finite element function space.

However, the finite element solution u_h given by (3.11), as is mentioned in the section 1, is probably defined on a highly irregular mesh introduced by L_h and $\mathfrak{T}_h(\Omega)$. To create a regular finite element approximation out of u_h, let $\mathfrak{T}_{h'}(\Omega)$ be a regular triangulation of Ω and let

$$(MRT) \quad \begin{cases} \bar{u}_{h'} \in \mathbb{U}_{h'}(\bar{u}_0;\ \Omega) \text{ be such that} \\ \bar{u}_{h'}(x_i) = u_h(x_i) - A\,x_i, \quad \text{if } x_i \text{ is a node of } \mathfrak{T}_{h'}(\Omega), \end{cases} \tag{3.12}$$

which is the interpolation of $u_h(x) - A\,x$ in $\mathbb{U}_{h'}(\bar{u}_0;\ \Omega)$. Now the function $u_{h'}(x) = \bar{u}_{h'}(x) + A\,x$ is a finite element approximation defined on a regular mesh introduced by $\mathfrak{T}_{h'}(\Omega)$ and the identity map $id \in T_{h'}(\Omega)$. We call the way of producing $(\bar{u}_{h'},\ id) \in \mathbb{U}_{h'}(\bar{u}_0;\ \Omega) \times T_{h'}(\Omega)$ from $(u, L) \in \mathbb{U}_h(\bar{u}_0;\ \Omega) \times T_h(\Omega)$ given by (3.11) and (3.12) the mesh regularization technique. By the standard finite element approximation theory [23] and the continuity and growth conditions of $f(\cdot)$, it is not difficult to show that

$$\lim_{h'\to 0} F(u_{h'};\Omega) = F(u_h;\Omega). \tag{3.13}$$

So $u_{h'}$ can be expected to be a good initial approximation for h' small. Most importantly, the mesh regularization technique helps to remove the extremely thin austenite needle tips remained in the martensite.

Lemma 3.1. *Let u_h be a solution of* (3.10)*. Suppose u_h has a thin austenite needle of width t_a in a pure variant of martensite. Let $u_{h'}(x) = \bar{u}_{h'}(x) + A\,x$ with $\bar{u}_{h'}(x)$ being given by* (3.12)*. Then, if h' is sufficiently small, the part of the needle with $t_a \ll h'$ will be removed from $u_{h'}$.*

Proof. Without loss of generality we may assume that the austenite needle in question is in a pure variant of martensite with deformation gradient U_0. Suppose the distance between the needle, which is denoted by N_a, and the other variant of the martensite is d which by assumption is greater than 0. Now, if $h' < d$, the elements in $T_{h'}(\Omega)$ pierced by the needle N_a must be completely separated from the other variant of the martensite. Suppose K is such an element where $t_a \ll h'$, the average deformation gradient of u_h on K can then be written as

$$\operatorname{meas}(K)\,\overline{\nabla u_h}|_K = \int_{K\setminus N_a} \nabla u_h(x)\,dx + \int_{K\cap N_a} \nabla u_h(x)\,dx.$$

By assumption ∇u_h is a good approximation of U_0 on $K \setminus N_a$, and it follows from $t_a \ll h'$ and the regularity of $T_{h'}(\Omega)$ that $\operatorname{meas}(K \cap N_a) \ll \operatorname{meas}(K \setminus N_a)$, so we have that $\overline{\nabla u_h}|_K$ is also a good approximation of U_0. Since $u_{h'}$ is the piecewise linear interpolation of u_h on the mesh $T_{h'}(\Omega)$, we have $\nabla u_{h'}|_K = \overline{\nabla u_h}|_K$. This implies the function $u_{h'}(x)$ approximates a pure martensite U_0 on K, and in particular the austenite needle is removed from K. $\square$

Lemma 3.2. *Let u_h be a solution of* (3.10)*. Suppose u_h has an austenite needle of width t_a located between two pure variants of a martensite laminate. Suppose the regular triangulation $T_{h'}(\Omega)$ is such that the interfaces of the martensite laminates are taken as mesh lines. Let $u_{h'}(x) = \bar{u}_{h'}(x) + A\,x$ with $\bar{u}_{h'}(x)$ being given by* (3.12)*. Then, if h' is sufficiently small, the part of the needle with $t_a \ll h'$ will be removed from $u_{h'}$.*

Proof. Suppose $K \in T_{h'}(\Omega)$ touches the needle N_a at the part with $t_a \ll h'$. Since the interface of the laminate is on a mesh line, the needle N_a is on the same mesh line too, thus K can only contain one of the variant of the martensite laminate. Without loss of generality we may assume the variant is U_0. The same argument as in the proof of lemma 3.1 completes the proof. $\square$

Remark 3.1. Since the simple laminate part of the microstructure is known in computation and it is not subject to change in the evolution, the condition in lemma 3.2 is easily satisfied. In addition, with the similar argument, it is easily shown that the conclusion of lemma 3.2 remains valid as long as the interfaces of the laminates are sufficiently close to the mesh lines.

Remark 3.2. In applying the mesh transformation method, we must keep in mind that the condition det $\nabla L > 0$ should always be satisfied. This condition at the ever shrinking austenite needles and other highly irregular shaped elements causes serious difficulties in the computation, since the step size is severely restricted in minimizing search process. As is proved in lemma 3.1 and lemma 3.2, the mesh regularization technique helps to remove the shrinking austenite needles, and in fact other highly irregular shaped elements as well, and thus overcomes this problem.

In applications, $\mathfrak{T}_{h'}(\Omega)$ is either taken to be $\mathfrak{T}_h(\Omega)$ or a refinement of it. In either case, $(\bar{u}_{h'},\ id)$ is taken as an initial data in searching for a minimizer of $F(u, L;\ \Omega)$ in $\mathbb{U}_{h'}(\bar{u}_0;\ \Omega) \times T_{h'}(\Omega)$.

The convergence analysis of the mesh transformation method combined with the mesh regularization technique $((MTM) + (MRT))$ is a more delicate issue and will not be discussed in this paper.

4. Numerical experiments and results

Let $\Omega = R(\frac{\pi}{4})\hat{\Omega}$, where $\hat{\Omega} = (-a,\ a) \times (-b,\ b)$ is a $2a \times 2b$ rectangular domain and

$$R(\alpha) = \begin{pmatrix} \cos\alpha & -\sin\alpha \\ \sin\alpha & \cos\alpha \end{pmatrix}$$

is a rotational matrix. Let $\mathfrak{T}_h(\Omega)$ be a family of regular triangulations defined by

$$\mathfrak{T}_h(\Omega) = \mathfrak{T}_h(R(\frac{\pi}{4})\hat{\Omega}) = \{R(\frac{\pi}{4})K : \forall K \in \mathfrak{T}_h(\hat{\Omega})\}, \tag{4.1}$$

where $\mathfrak{T}_h(\hat{\Omega})$, for $h = h_{N,M} = \frac{2}{N\cdot M}\sqrt{(aM)^2 + (bN)^2}$ with $N \geq 2$ and $M \geq 2$, is a family of regular triangulations of $\hat{\Omega}$ introduced by the lines

$$\begin{cases} y = & -b + \frac{2b}{M}i, & 0 \leq i \leq M; \\ x = & -a + \frac{2a}{N}j, & 0 \leq j \leq N; \\ y = & \frac{Nb}{Ma}(x+a) + b - \frac{4b}{M}k, & 0 < k < \frac{M+N}{2}; \\ y = & \frac{-Nb}{Ma}(x-a) - b + \frac{4b}{M}k, & 0 < k < \frac{M+N}{2}. \end{cases} \tag{4.2}$$

Let $\partial\Omega_{\pm} = R(\pi/4)\{(\pm a,\ y) \in \partial\hat{\Omega} : -b < y < b\}$, and let

$$\partial\Omega_0(\theta) = \{(x,y) \in \partial\Omega \setminus (\partial\Omega_+ \cup \partial\Omega_-) : \theta(x,y) \leq \theta_T\} \tag{4.3}$$

where θ_T is the transformation temperature and $\theta(x, y)$ is a temperature distribution defined on Ω. In our numerical simulations, the length and width of Ω are set to be $2a = 2$ and $2b = 1$ and $\theta(x, y)$ is a linear temperature distribution given by

$$\theta(x, y) = \frac{\theta_+ + \theta_-}{2} + \frac{\theta_+ - \theta_-}{2\sqrt{2}a}(x + y), \quad \forall (x, y) \in \bar{\Omega} \tag{4.4}$$

which takes values $\theta_\pm$ on $\partial\Omega_\pm$,

In the following numerical experiments, we make numerical simulations on the austenitic-martensitic phase transition and the propagation of the austenite-finely twinned martensite interface by using the mesh transformation and regularization method $((MTM)+(MRT))$ given in section 2 to solve the problem of minimizing the elastic energy

$$F(u;\ \Omega) = \int_\Omega f(\nabla u(x),\ \theta(x))\, dx \tag{4.5}$$

in the set of admissible functions

$$\mathbb{U}(A_\lambda^-;\ \Omega) = \{u \in W^{1,p}(\Omega; R^2) : u(x) = A^- x, \text{ on } \partial\Omega_0(\theta)\}, \tag{4.6}$$

where in (4.5) $f(\nabla u,\ \theta) = \phi(C,\ \theta)$ is defined by (2.4)-(2.7) with

$$\begin{cases} d_0 = 500, \quad e = 3.5, \quad g = 15, \quad \hat{\varepsilon} = 0.05, \\ \alpha = \frac{2.02}{\pi}, \ \mu = 0.25, \ \gamma = 0, \end{cases} \tag{4.7}$$

and where in (4.6) $A_\lambda^- = (1-\lambda)U_0 + \lambda R^- U_1$ (see (2.15) and (2.16)) which admits a laminated microstructure oscillating between U_0 and $R^- U_1$ with volume fraction $1 - \lambda$ and λ (*c.f.* [1, 10]). The numerical results of microstructures will be shown in the physical configuration with

$$(x_1, y_1)^T = R(\arctan \frac{u_h^2(a, -b) - u_h^2(-a, -b)}{u_h^1(a, -b) - u_h^1(-a, -b)})(u_h^1(x, y), u_h^2(x, y))^T,$$

where an element is pained white, black or grey according to whether it is closer to $SO(2)U_0$, $SO(2)R^- U_1$ or $SO(2)$ respectively. It should be noticed that in the figures the scale in x_1 direction is twice as large as the one in y_1 direction, so the needles are actually thinner and sharper than they appear in the figures.

Example 1. Let $\theta_- = 64\ ^\circ\mathrm{C}$ and $\theta_+ = 78\ ^\circ\mathrm{C}$, and let the volume fraction $\lambda = 0.5$. We take initially $N = 8$ and $M = 16$, set the initial value of the mesh transformation map $L_0 = id$ (see (3.7)), and set the initial value of $\hat{u}_h^0$ to be a random perturbation with $|\hat{u}_h^0|_\infty \leq 2.0 \times 10^{-3}$.

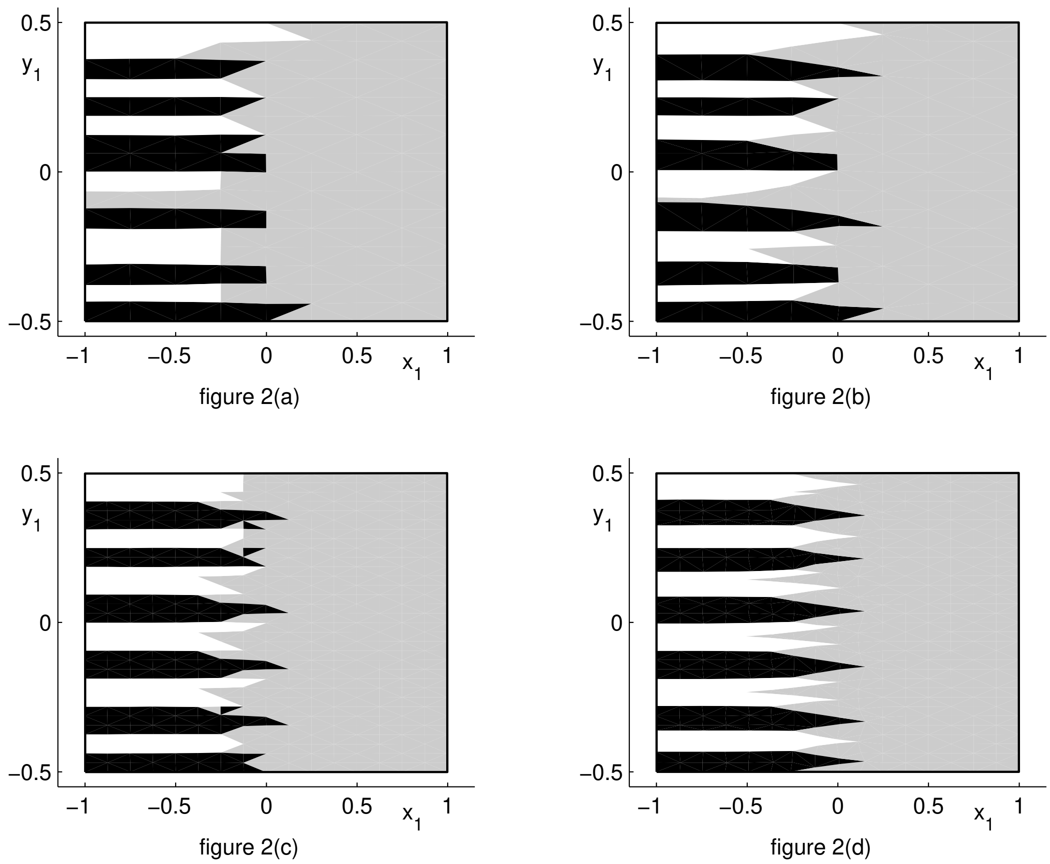

FIGURE 2. The procession of the mesh transformation method equipped with the mesh regularization technique in obtaining an austenite-finely twinned martensite phase transition.

The conjugate gradient method combined with a linear search is applied to solve the discrete problem (MTM) (see (3.10)). The numerical results of the mesh transformation method equipped with the mesh regularization technique are shown in figure 2(a)-(d). Figure 2(a) shows the numerical result of the algorithm in which the mesh transformation map L is kept identity, that is without using the mesh transformation method, the elastic energy so obtained is -0.1752×10^{-3}. Then we allow the mesh to be deformed by applying the mesh transformation method, which reduces the elastic energy to -0.2182×10^{-3} and produces Figure 2(b). Compare the two pictures, it is clearly seen that by applying the mesh transformation method the defect area in the twinned martensitic phase in Figure 2(a) is squeezed into a narrow gap in Figure 2(b). Now we apply the mesh regularization technique by interpolating the numerical solution on a refined mesh given by (4.2) with $N = 16$ and $M = 32$ (see (3.12) where A is set to A_λ^-), and taking the interpolating function as the initial data, we apply the conjugate gradient method combined with a linear search to solve (MTM) on the refined mesh. Figure 2(c) shows the numerical result obtained by setting $L \equiv id$ and the elastic energy in this case is reduced to -0.2463×10^{-3}. Further optimization by allowing the mesh to be deformed reduces the energy further to -0.2815×10^{-3} and the numerical result is shown in Figure 2(d). To get better numerical approximations, the mesh can be further refined. However, it does not seem proper to apply the mesh regularization technique in this case, since the mesh is not highly irregularly deformed except in a neighborhood of the austenite-finely twinned martensite interface where the needles form, and an application of the technique without sufficiently refining the mesh may blunt the needles. In fact, numerical experiments showed that a direct mesh refinement produces sharper numerical result. For the cases of $N = 32$, $M = 64$ and $N = 64$, $M = 128$, the algorithm produces pretty much the same picture as Figure 2(d) and reduces the elastic energy to -0.2845×10^{-3} and -0.2858×10^{-3} respectively which indicates the convergence of the method. An important observation of the computations on the refined meshes is that the needles are stable in the sense that they do not branch into thinner needles without sufficiently large perturbations.

Example 2. Let $\lambda = 0.5$, and let $N = 16$ and $M = 32$. Let the initial temperature be given by $\theta_- = 64\ ^\circ\mathrm{C}$ and $\theta_+ = 78\ ^\circ\mathrm{C}$, and take the numerical result shown in Figure 2(d) as the initial finite element approximation. We apply the mesh transformation method equipped with the mesh regularization technique to numerically simulate the growth of the needle-like microstructures and the propagation of the austenite-finely twinned martensite interface by varying the temperature by increments.

The numerical results of the simulation are shown in Figure 3(a)-(d). It is interesting to notice that the mesh regularization technique is applied without mesh refinement in these cases. Figure 3(a) is obtained by increasing θ_- from $64\ ^\circ\mathrm{C}$ to $67\ ^\circ\mathrm{C}$ while maintaining θ_+ unchanged, we see that the interface moves accordingly to the left and the elastic energy rises to -0.6034×10^{-4}. Figure 3(b) is obtained by decreasing θ_+ from $78\ ^\circ\mathrm{C}$ to $76\ ^\circ\mathrm{C}$ while maintaining θ_- unchanged, we see that the interface moves accordingly to the right with the elastic energy being reduced to -0.3391×10^{-3}. By further decreasing θ_+ from $76\ ^\circ\mathrm{C}$ to $74\ ^\circ\mathrm{C}$

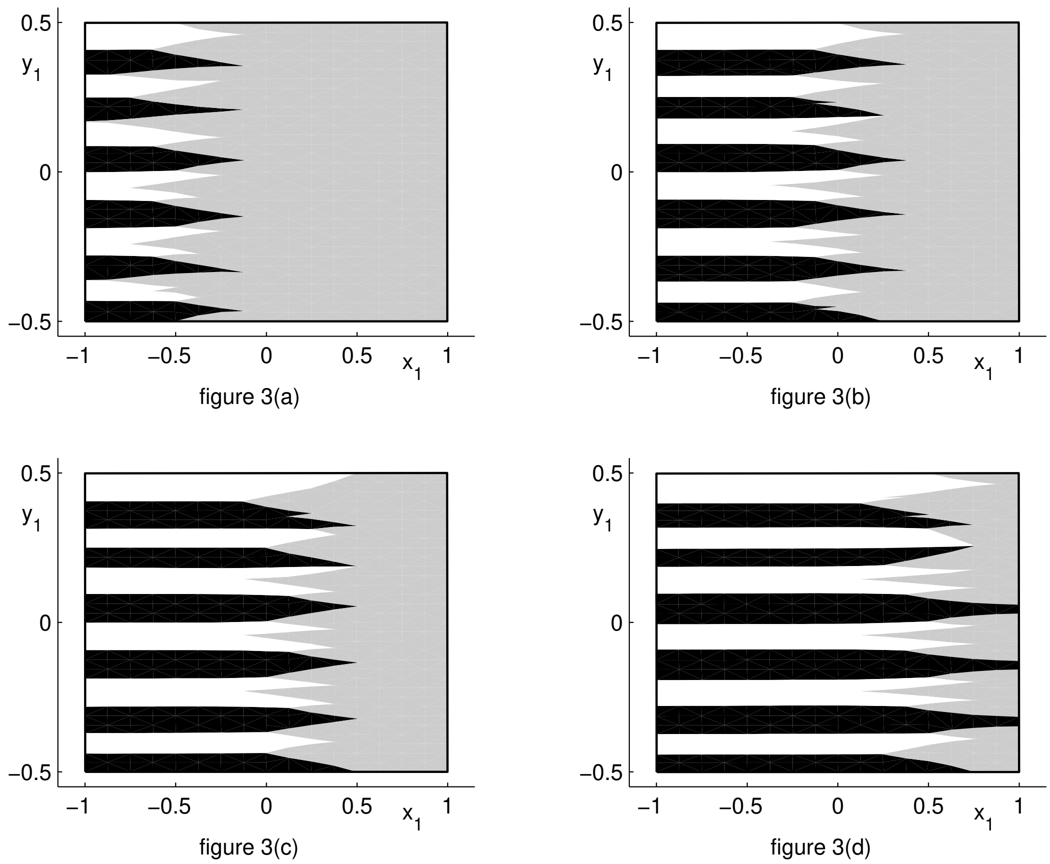

FIGURE 3. The growth of the needle-like microstructures and the propagation of the austenite-finely twinned martensite interface.

and then to 72 °C while keeping θ_- unchanged, and by applying the mesh transformation method combined with the mesh regularization technique successively, the needle-like microstructures and the austenite-finely twinned martensite interface moves continually to the right and the elastic energy drops to -0.4095×10^{-3} and -0.5367×10^{-3} respectively.

In comparison with the mesh transformation method without using the mesh regularization technique, of which the numerical results corresponding to the cases with respect to Figure 3(a)-(d) are shown in Figure 4(a)-(d), we see that the mesh transformation method combined with the mesh regularization technique produces much sharper numerical results, since the relative errors for the volume ratio of the austenitic phase to the martensitic phase are 43.2%, 14.0%, 37.7% and 184% for the numerical results shown in Figure 4(a)-(d) and are 3.05%, 3.81%, 2.86% and 6.01% for the numerical results shown in Figure 3(a)-(d). Furthermore

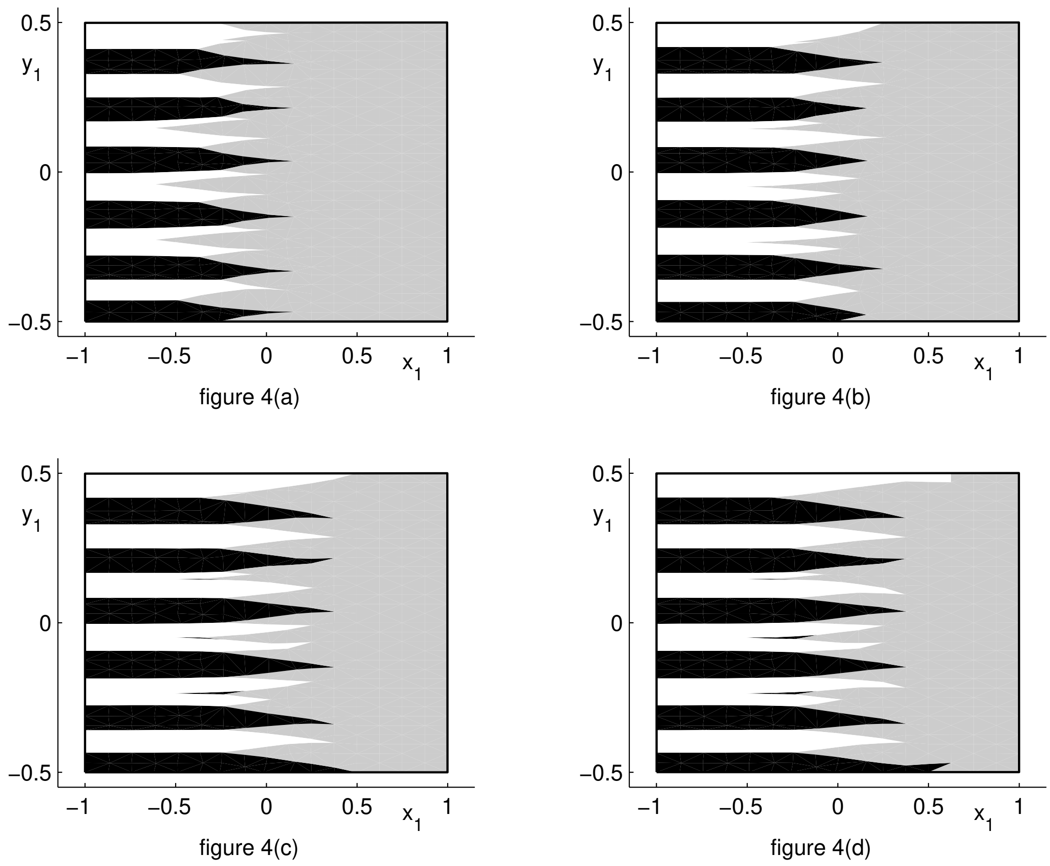

FIGURE 4. The numerical results obtained without using the mesh regularization technique.

it is also found that the mesh transformation method combined with the mesh regularization technique converges faster. This can be explained by the fact, as is clearly shown in Figure 4, that some of the austenite needles shrink almost into line segments and the minimizing procedure keeps on the shrinking process with increasingly smaller step size which finally causes the termination of the minimizing search. Another advantage of the mesh regularization technique is that the perturbation introduced by the mesh regularization helps to break the energy barrier and that the problem defined on the regularized mesh is better conditioned for the propagation of the needle-like microstructures. The effect is more significant if the mesh is finer.

Even though the mesh used in the above numerical experiments is very coarse, the numerical results obtained are satisfactory. For example, the volume average of the relative errors of the volume fractions of the numerical approximations shown in Figure 2(d) and Figure 3(a)-(c) are around 2%. It is also interesting to notice that in Figure 3(d), some of the needles grow longer than expected and reach the boundary, this might be explained by the fact that the distance between the expected needle tips to the boundary is already much less than the length scale of the austenite-finely twinned martensite interface region and the boundary effect shows its power.

References

[1] J. M. Ball and R. D. James, *Fine phase mixtures as minimizers of energy.* **Arch. Rat. Mech. Anal., 100**(1987)1, 13-52.

[2] J. M. Ball and R. D. James, *Proposed experimental test of a theory of fine microstructure and the two-well problem.* **Phil. Trans. R. Soc. London 338A**(1992), 389-450.

[3] M. Chipot and D. Kinderlehrer, *Equilibrium configurations of crystals*, **Arch. Rat. Mech. Anal., 103**(1988)1, 237-277.

[4] D. Kinderlehrer, *Remarks about equilibrium configurations of crystals*, in **Material Instabilities in Continuum Mechanics and Related Problems**, J. M. Ball, ed., Oxford University press, 1987, pp. 217-242.

[5] C. Collins and M Luskin, *The computation of the austenitic-martensitic phase transition.* In **Partial Differential Equations and Continuum Models of Phase Transitions** Lecture Nodes in Physics, Vol. 344, M. Rascle, D. Serre and M. Slemrod, eds, Springer-Verlag, New York, (1989), pp. 34-50.

[6] C. Collins, *Computation of twinning*, in **Microstructure and Phase Transitions**, IMA Volumes in Mathematics and Its Applications, Vol.54, J. Ericksen, R. James, D. Kinderlehrer and M. Luskin, eds, Springer-Verlag, New York, (1993), pp. 39-50.

[7] C. Collins, M. Luskin and J. Riordan, *Computational results for a two-dimensional model of crystalline microstructure*, in **Microstructure and Phase Transitions**, IMA Volumes in Mathematics and Its Applications, Vol.54, J. Ericksen, R. James, D. Kinderlehrer and M. Luskin, eds, Springer-Verlag, New York, (1993), pp. 51-56.

[8] P. Gremaud, *Numerical optimization and quasiconvexity*, **Euro. J. Appl. Math., 6**(1995) 69-82.

[9] P. Pedregal, *On the numerical analysis of non-convex variational problems*, **Numer. Math., 74**(1996), 325-336.

[10] M. Luskin, *On the computation of crystalline microstructure.* **Acta Numerica, 5**(1996), 191-257.

[11] R. A. Nicolaides, N. Walkington and H. Wang, *Numerical methods for a nonconvex optimization problem modeling martensitic microstructure.* **SIAM J. Sci. Comput., 18**(1997), 1122-1141.

[12] Z.-P. Li, *Simultaneous numerical approximation of microstructures and relaxed minimizers.* **Numer. Math., 78** (1997), 21-38.

[13] Z.-P. Li, *Laminated microstructure in a variational problem with a non-rank-one connected double well potential*, **J. Math. Anal. Appl., 217**(1998), 490-500.

[14] Z.-P. Li, *Rotational transformation method and some numerical techniques for the computation of microstructures.* **Math. Models Meth. Appl. Sci., 8**(1998), 985-1002.

[15] C. R. Collins, *Convergence of a reduced integration method for computing microstructures.* **SIAM J. Numer. Anal., 35**(1998), 1271-1298.

[16] Z.-P. Li, *A mesh transformation method for computing microstructures.* To appear in **Numer. Math.**.

[17] Z.-P. Li, *A periodic relaxation method for computing microstructures.* **Appl. Numer. Math., 32**(2000), 291-303.

[18] Z.-P. Li, *Finite order rank-one convex envelopes and computation of microstructures with laminates in laminates.* BIT, 40(2000), 745-761.

[19] Z.-P. Li, *Computations of needlelike microstructures*, Research Report No.57, Institute of Mathematics and School of Mathematical Sciences, Peking University, 1999.

[20] J.M. Ball, *A version of the fundamental theorem for Young measures.* In **Partial Differential Equations and Continuum models of Phase Transitions**, Lecture Notes in Physics, No. 344, M. Rascle, D. Serre and M. Slemrod, eds., Springer-Verlag, New York (1989), pp. 207-215.

[21] P. Klouček and M. Luskin, *The computation of the dynamics of the martensitic transformation, Continuum Mech. Thermodyn., 6*(1994), 209-240.

[22] P. G. Ciarlet, **Mathematical Elasticity**, Volume 1: Three Dimensional Elasticity. North-Holland, Amsterdam, 1988.

[23] P.G. Ciarlet, **The Finite Element Method for Elliptic Problems**. North-Holland, Amsterdam, 1978.

E-mail address: `zpli@math.pku.edu.cn`